Damage effect and mechanism of the GaAs high electron mobility transistor induced by high power microwave*

Yang Liu(刘阳)[1,†], Chang-Chun Chai(柴常春)[1], Yin-Tang Yang(杨银堂)[1], Jing Sun(孙静)[2], and Zhi-Peng Li(李志鹏)[2]

[1] *Ministry of Education Key Laboratory of Wide Band-Gap Semiconductor Materials and Devices, Xidian University, Xi'an* 710071, *China*
[2] *Space Payload System Innovation Center, China Academy of Space Technology, Xi'an* 710100, *China*

(Received 2 December 2015; revised manuscript received 26 December 2015; published online 25 March 2016)

In this paper, we present the damage effect and mechanism of high power microwave (HPM) on AlGaAs/GaAs pseudomorphic high-electron-mobility transistor (pHEMT) of low-noise amplifier (LNA). A detailed investigation is carried out by simulation and experiment study. A two-dimensional electro-thermal model of the typical GaAs pHEMT induced by HPM is established in this paper. The simulation result reveals that avalanche breakdown, intrinsic excitation, and thermal breakdown all contribute to damage process. Heat accumulation occurs during the positive half cycle and the cylinder under the gate near the source side is most susceptible to burn-out. Experiment is carried out by injecting high power microwave into GaAs pHEMT LNA samples. It is found that the damage to LNA is because of the burn-out at first stage pHEMT. The interiors of the damaged samples are observed by scanning electron microscopy (SEM) and energy dispersive spectrometer (EDS). Experimental results accord well with the simulation of our model.

Keywords: low noise amplifier, HEMT, high power microwave, damage effect

PACS: 85.30.Tv, 84.40.–x **DOI:** 10.1088/1674-1056/25/4/048504

1. Introduction

With the rapid development of high power microwave (HPM) source generation technology, growing attention has been paid to the threat posed by intentional electromagnetic interference (IEMI).[1–7] Such an HPM induced by IEMI could couple into the interior electronics of a system through two generic ways, i.e., front-door coupling and the back-door coupling, which could disrupt or destroy a device. The effect of man-made electromagnetic interferences on electronic systems is an ongoing and wide research topic.[7–10]

The malfunction/destruction failure rate (M/D FR) was measured to investigate the susceptibility of LNA due to front-door coupling under narrow-band high power electromagnetic wave.[11] Experimental measurements of susceptibility of electronics to HPM and UWB irradiation with repetition rate signals were presented in Ref. [12]. The injecting method was adopted to study the microwave vulnerability effect of integrated circuits (ICs) in Ref. [10]. Experimental results from the radiation method of microwave pulses effect in L band on personal computer (PC) were presented in Ref. [13]. The HPM induced latch-up effect on complementary metal–oxide semiconductors (CMOS) have been studied in Ref. [14]. A theoretical study of the EMP damage mechanism and the susceptibility trend of pulse parameter-dependent are discussed in Refs. [15]–[18].

As for an electric system, LNA is a key element in RF front-end of the wireless receiver, which is generally the most sensitive section at the same time. Owing to the potential application to high breakdown voltage, low on-resistance and high frequency, AlGaAs/GaAs pseudomorphic high-electron-mobility transistor (pHEMT) gradually serves as the core element in LNA. In previous studies, the burnout characteristics of GaAs MESFET were studied in Refs. [19] and [20]. In Ref. [21], four types of defects on damaged GaAs HEMT MMIC were analyzed. The degradation effect of GaAs pHEMT induced by HPM was discussed in Ref. [22]. The burnout properties of the GaAs pHEMT was analyzed in Ref. [23]. However, the study mentioned above placed emphasis on the experimental study, theoretical research was not sufficient, it needs further studying.

This paper focuses on the damage effect of pHEMT induced by front-door coupling HPM. Firstly, a two-dimensional (2D) electro–thermal model of a typical pHEMT is established with the device simulator Sentaurus-TCAD. Secondly, the damage process and physical mechanism are simulated. The variations of device internal electric field, the current density and the temperature distributions with time are analyzed. Finally, an experiment is carried out by injecting HPM into LNA, and the characteristics of damage morphology are analyzed by using scanning electron microscopy (SEM). The energy dispersive spectrometer (EDS) is used to analyze elemental composition at the location of burn-out.

*Project supported by the National Basic Research Program of China (Grant No. 2014CB339900) and the Open Fund of Key Laboratory of Complex Electromagnetic Environment Science and Technology, China Academy of Engineering Physics (Grant No. 2015-0214.XY.K).

†Corresponding author. E-mail: yyliu1987@163.com

© 2016 Chinese Physical Society and IOP Publishing Ltd

2. Structure and model

2.1. Structure

Figure 1 illustrates the 2D view of the simulated δ-doped AlGaAs/GaAs pHEMT. As depicted in Fig. 1, the structure under investigation consists of semi-insulating GaAs substrate, InGaAs channel, AlGaAs spacer with a δ-doping layer inside, GaAs cap layer and Si_3N_4 passivation layer. The distances of source-to-gate and gate-to-drain are both 0.5 μm. The gate length is 0.15 μm. The mole fractions of $Al_xGa_{1-x}N$ and $In_{1-y}Ga_y$ are kept to be 0.30 and 0.75, respectively.

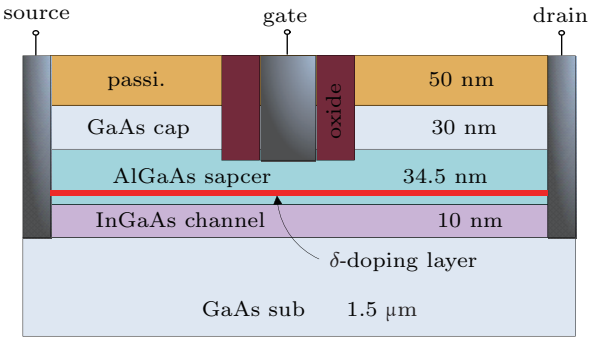


Fig. 1. (color online) Structure of the single delta-doping GaAs pHEMT.

2.2. Numerical modeling

To investigate the damage effect, the advanced mixed mode device and circuit on GaAs pHEMTs is simulated by using Sentaurus-TCAD. The presence of high current and high voltage causes a huge joule heat within the device, which may lead to a sharp rise in temperature during the injection of HPM. Hence the nonuniform temperature distribution and heat diffusion are major concerns. For crystalline materials, they need many thermo-related parameters to describe the thermodynamic behavior among which lattice thermal conductivity and specific heat are the two most important parameters. Both of them are susceptible to temperature variation, hence they cannot be regarded as constant any more when temperature increases. The fitting curve (line) used in the simulation on the basis of the experiment data[24,25] (scatter plot) is shown in Fig. 2. The fitting curve follows the following equations:

$$C(T) = 1.61 + 2.08 \times 10^{-4} T + 7.96 \times 10^{-9} T^2, \quad (1)$$

$$\kappa(T) = 0.67 - 9.75 \times 10^{-4} T + 3.89 \times 10^{-7} T^2. \quad (2)$$

The theoretical calculation and the experimental results have shown that the inductive voltage coupling from front-door is damped sinusoidal voltage.[26] Therefore, the voltage source used in simulation can be simplified as follows:

$$V_{\mathrm{HPM}} = \begin{cases} V_0 \dfrac{t}{t_1} \sin(2\pi f_0 t), & 0 < t < t_1, \\ V_0 \sin(2\pi f_0 t), & t_1 < t, \end{cases} \quad (3)$$

where V_0 is the voltage amplitude, t_1 is the rise time of the pulse, and f_0 is the carrier frequency.

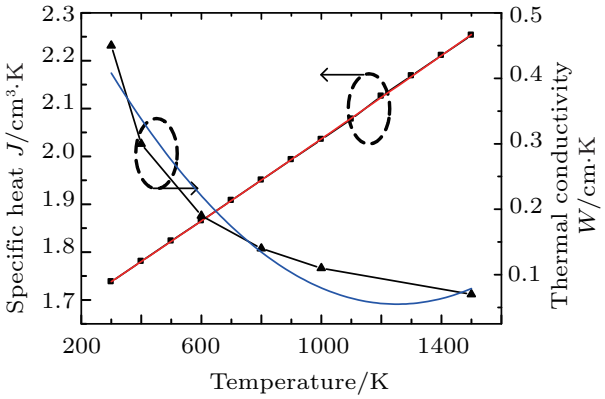


Fig. 2. (color online) Variation trends of lattice thermal conductivity and specific heat with lattice temperature increasing.

Additionally, there are a number of physical models used in simulation such as mobility degradation in high electric field, avalanche generation effect and self-heating effect. Since the drift-diffusion approach often overestimates the ionization generation rate, the hydrodynamic model is employed to provide a better accuracy. For the numerical expression of the physical model mentioned above, it can be seen in Ref. [27]. Here, we will not go into details of them.

3. Result and discussion

For the transistor shown in Fig. 1, HPM with a voltage of 13 V, frequency of 1 GHz, and rise time of 0 ns, is injected into the gate terminal. At the same time, the transistor is biased at the operating voltage that the drain voltage is 2 V and the source is grounded. The analyses of the damage effect and mechanism based on the temperature increasing within device are presented as follows. Figure 3 shows the dependence of temperature increasing with time during burn-out process.

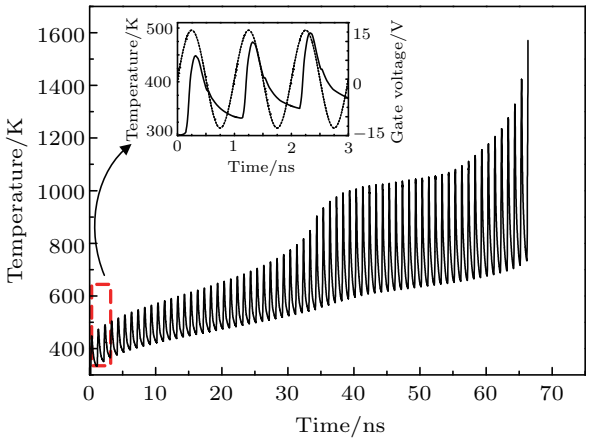


Fig. 3. (color online) Variation of maximum temperature within device with time.

It can be seen that the maximum temperature within device keeps increasing under the action of microwave, and fi-

nally rises up to the 1511 K (GaAs melting point) at the 66th period. The variation of temperature in the first three periods is illustrated in the inset. It indicates that the temperature behaves as periodical increasing–decreasing–increasing. It increases during positive half cycle and then decreases during negative half cycle. To explain this phenomenon, the current density and electric field at 0.25 ns and 0.75 ns are shown in Fig. 4, respectively.

According to Fig. 4, the electric field increases quickly soon after the microwave injecting into the gate electrode and exceeds the critical electric field required by impact ionization (1.75×10^5 V/cm, Fig. 4(a)). Plenty of carriers are produced due to avalanche generation and then float to the electrode immediately through the channel which is turned on during positive half cycle. It will lead to the increase of current density as shown in Fig. 5(a).

During the negative cycle, the Schottky junction is reverse-biased. Therefore, the current density is extremely low (Fig. 5(b)). Massive electrons generated by avalanche breakdown cannot be transferred immediately, thus they will be accumulated at the channel under the gate. Electric potential difference resulting from accumulated electrons causes the electric field to be a little higher than the electric field in positive half cycle (Fig. 4(b)). According to the power density $P = J \cdot E$, the temperature depends on current density and electric field. Therefore, based on the prominent difference dominated by current density, an amount of heat will be generated and accumulated during the positive half cycle.

It is also indicated that the overall temperature increase shows that the temperature sudden rises twice, in which the first time rising is at 32 ns and the second time rising is at 64 ns. A detailed investigation of the damage process is performed by analyzing the variations of the electric field, the current density and the temperature in the device with time.

3.1. Variation of the current density with time

Figure 6(a) illustrates the variations of overall current density of three electrodes with time till burn-out.

Figure 6 shows that the gate current density is about 0.014 A, but then decreases slightly because carrier mobility contributed by lattice scattering decreases as the temperature increases. As temperature rises up to 750 K, the current increases sharply and reaches above 0.02 A. This is because 750 K is the threshold temperature for intrinsic excitation of GaAs.[28] In this case, the device cannot operate properly and the repairable damage may occur.

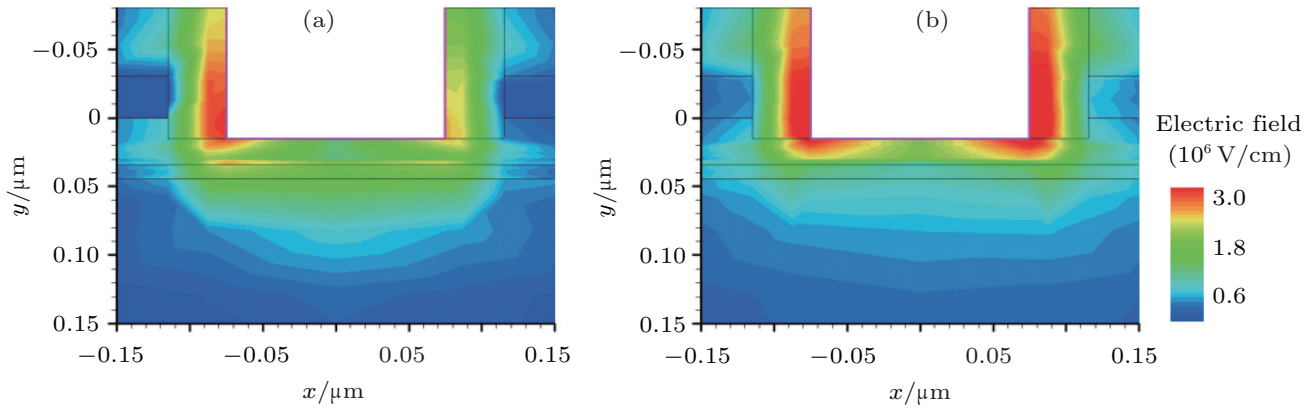


Fig. 4. (color online) Distributions of electric field at (a) 0.25 ns and (b) 0.75 ns.

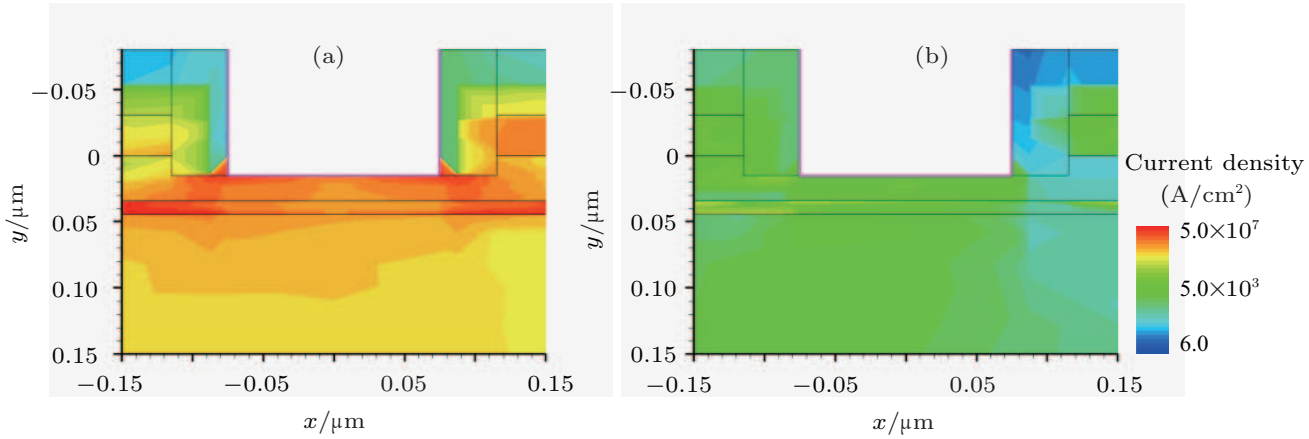


Fig. 5. (color online) Distributions of current density at (a) 0.25 ns and (b) 0.75 ns.

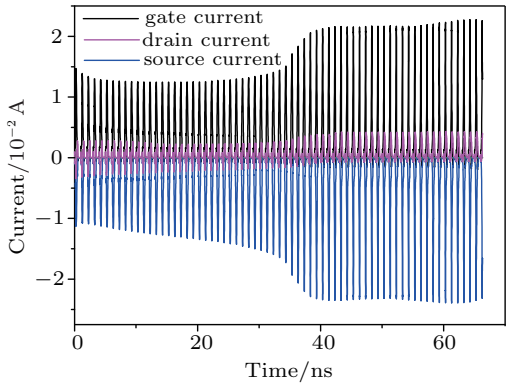


Fig. 6. (color online) Variations of of current density at gate (black), source (blue), and drain (red) electrode with time.

Figure 7 shows the distributions of current density before (0.25 ns) and after (0.75 ns) intrinsic excitation, respectively. It can be found that conduction channel is formed from the gate electrode near source and drain side to the two-dimensional electron gas (2DEG) channel under high electric field. Current mainly flows from gate to the source through the 2DEG channel at the interface of heterostructureas as shown in Fig. 7. After intrinsic excitation, a large number of electrons flow from the gate to the 2DEG channel, which causes the gate current to be kept to be about 0.02 A. It indicates that the maximum current density is located beneath gate near the source side.

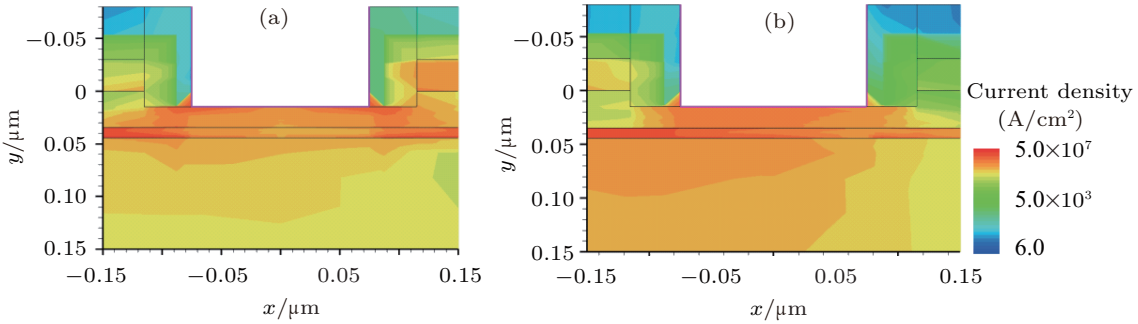


Fig. 7. (color online) Distributions of current density at (a) 0.25 ns and (b) 50.25 ns.

3.2. Variation of the electric field with time

In order to study the electric field distributions during the damage process, electric field at four typical moments: 0.25 ns, 35.25 ns, 50.25 ns, and 66 ns, are selected. Figure 8 shows the distributions of the electric field at different moments. Based on the curvature effect and the potential difference, the maximum electric field is located at the cylinder beneath the gate near the source side at 0.25 ns (Fig. 8(a)). The electric field increases slightly as time goes on. This is because the electric field has strong dependence on the carrier transport velocity which will decrease with the increase of temperature (Fig. 8(b)). With the heat accumulation, when the temperature ascends to 1200 K, massive electrons will be produced by thermal breakdown, but electrons, restricted by carrier transport ability, will accumulate under the gate instead of transferring to electrodes, which will cause the electric field to rise sharply (Fig. 8(d)).

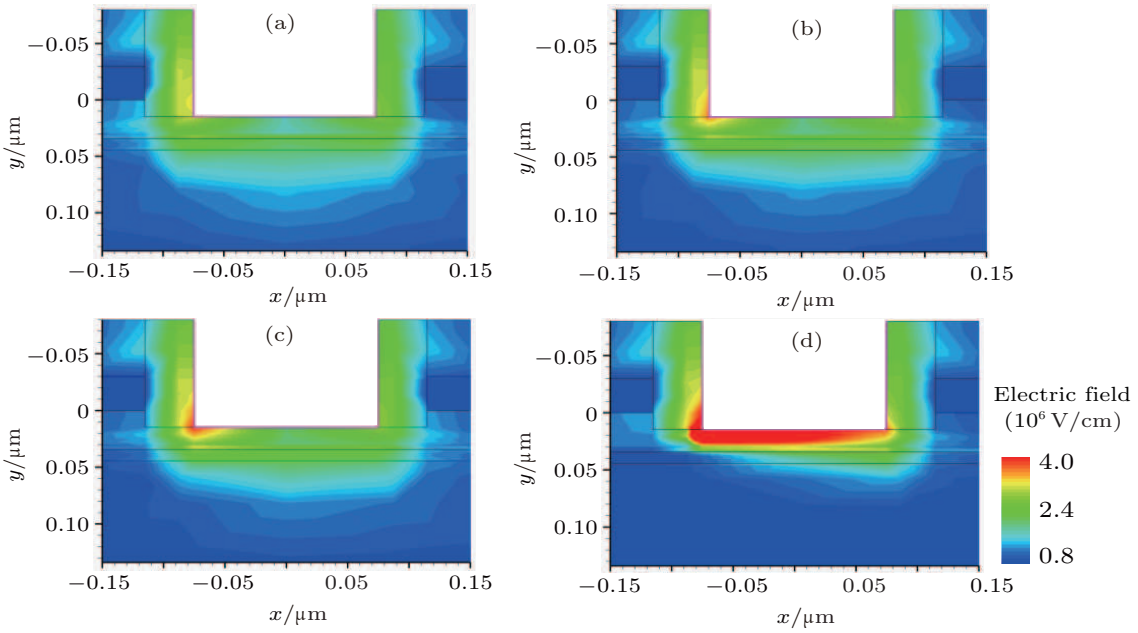


Fig. 8. (color online) Distributions of electric field at (a) 0.25 ns (b) 35.25 ns (c) 50.25 ns, and (d) 66.25 ns.

3.3. Variation of the temperature with time

From the above discussion, it follows that under the joint action of electric field and current density, the increase of current is the leading factor for the first sudden rise of temperature which is induced by intrinsic excitation. With the heat accumulation, a positive feedback is formed between the heat accumulation and the thermal breakdown when the temperature is equal to or greater than 1200 K. It will cause the electric field to increase immediately, and it will also causes the temperature to increase till burn-out. Figure 9 shows the temperature distribution at burn-out. It can be seen that the most heat accumulates at the cylinder under the gate near the source side and the cylinder is most susceptible to burn-out.

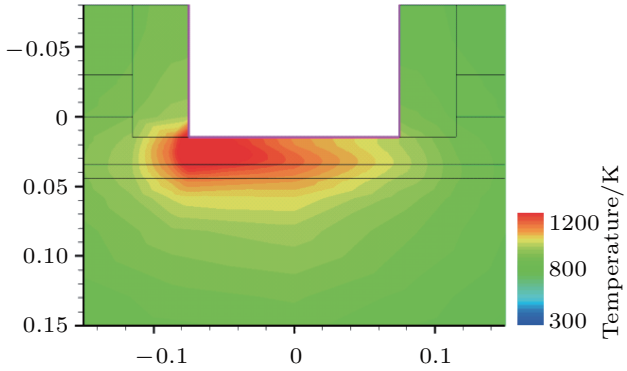


Fig. 9. (color online) Distribution of electric field at burn-out.

4. Comparison with experimental results

In order to verify the previous explanations, experiment is performed by directly injecting microwave power into LNA sample which consists of two GaAs pHEMTs: one is the first stage (numbered as 11#) and the other is the second stage (numbered as 1-2#). The injected HPM signals are continuous waves with high density power. The noise figure of LNA deteriorating by 20 dB is determined as a damage criterion.[29]

The DC characteristic is tested on two pHEMT samples. Sample 1-1# shows short character, and the sample 1-2# shows the junction feature. It can be inferred that the damage of the first stage is responsible for the failure of LNA. Further research about the HPM damage effect is carried out by using SEM to observe the interior of the sample 1-1#.

From the interior features of sample #1-1 characterized by SEM, it can be seen that, the gate-to-source channel is obviously overheating and burned and one or more molten globules and pits emerge between the source and gate contact (see Fig. 10). The damage location shows accordance with the experimental results discussed in Ref. [23]. The EDS is used to make elemental analysis at burn-out spot and region A in Fig. 10. Diagram of ESD is shown in Fig. 11. It is found that the spot of burn-out region contains higher As-element. So the inference above is confirmed that part of gate metal is melted and splashes out.

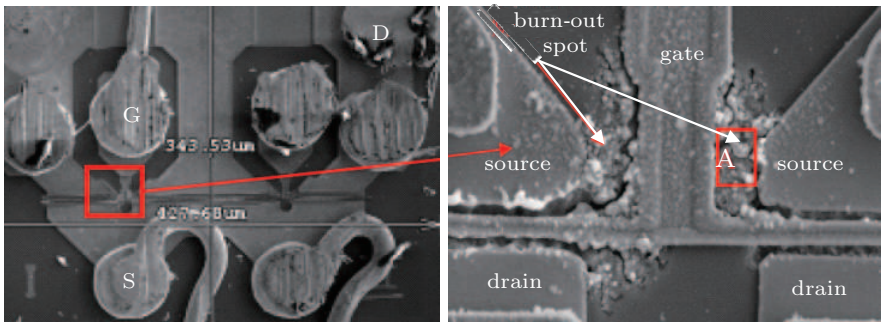
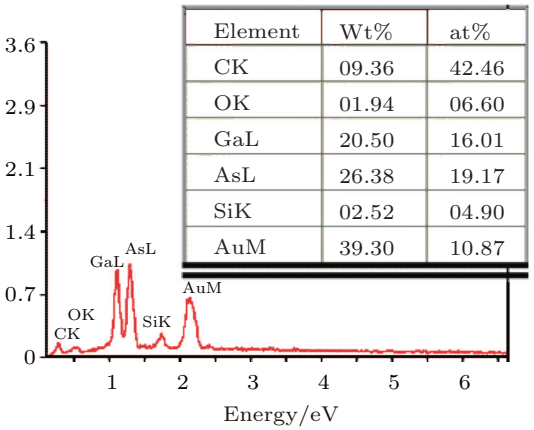


Fig. 10. (color online) Interior features of sample #1-1 characterized by SEM.



Element	Wt%	at%
CK	09.36	42.46
OK	01.94	06.60
GaL	20.50	16.01
AsL	26.38	19.17
SiK	02.52	04.90
AuM	39.30	10.87

Fig. 11. (color online) Diagram of energy spectrum of region A.

5. Conclusions and perspectives

In this paper we investigate the damage effect of HPM on a two-stage LNA which consists of GaAs pHEMTs. A typical δ-doped pHEMT induced by the pulsed microwaves is established with the device simulator Sentaurus-TCAD by considering the mobility degradation in high electric field, avalanche generation effect and self-heating effect. According to the analyses of the variations of device internal distributions of the electric field, the current density and the temperature with time, it is predicted that the cylinder under gate near the source side is most susceptible to damage. Experimental result shows that the damage to GaAs pHEMT at first stage is responsible for the failure of LNA. The damage to GaAs pHEMT is be-

cause of the burn-out of gate metal. Observations by SEM and EDS confirm that the gate metal is melted and forms molten globule, which is consistent with the simulation results.

Acknowledgment

We thank the Xi'an Institute of Space Radio Technology (CAST Xi'an) for the financial and technical assistance.

References

[1] Ren Z, Yin W Y Shi Y B and Liu Q H 2010 *IEEE Trans. Electron Dev.* **57** 345
[2] Kim Kand Iliadis A A 2010 *Solid-State Electron.* **54** 18
[3] Iliadis A Aand Kyechong K 2010 *IEEE Trans. Dev. Mater. Reliab.* **10** 347
[4] Mansson D, Thottappillil R, Nilsson T, Lunden O and Backstrom M 2008 *IEEE Trans. Electromagn. Compat.* **50** 434
[5] Kim K and Iliadis A A 2008 *Solid-State Electron.* **52** 1589
[6] Nitsch D, Camp M, Sabath F, ter Haseborg J L and Garbe H 2004 *IEEE Trans. Electromagn. Compat.* **46** 380
[7] Sabath F 2008 *Poceedings of the* 29*th General Assembly of the URSI*, 2008, Chicago, USA, p. 50 101
[8] Brauer F, Sabath F. terHaseborg J L 2009 *IEEE International Symposium on the Electromagnetic Compatibility*, 2009, Piscataway, NJ, USA
[9] Fang J Y, Shen J A, Yang Z Q and Qiao D J 2003 *High Power Laser and Particle Beams* **15** 591 (in Chinese)
[10] Palisek L and Suchy L 2009 *Proceeding of the* 17*th IEEE International Pulsed Power Conference*, 2009, Washington, DC, USA, p. 1244
[11] Backstrom M G and Lovstrand K G 2004 *IEEE Trans. Electromagn. Compat.* **46** 396
[12] Klunder C and Haseborg J L 2010 *IEEE International Symposium on the Electromagnetic Compatibility*, 2010, p. 359
[13] Liu C J, Yan L P, Fan R D, Luo J and Pu T L 2007 *High Power Laser and Particle Beams* **19** 1580 (in Chinese)
[14] Yu X H, Chai C C, Ren X R, Yang Y T, Xi X W and Liu Y 2014 *J. Semicond.* **35** 084011
[15] Ma Z Y, Chai C C, Ren X R, Yang Y T and Chen B 2012 *Acta Phys. Sin.* **61** 078501 (in Chinese)
[16] Ma Z Y, Chai C C, Ren X R, Yang Y T Chen B and Zhao Y B 2012 *Chin. Phys. B* **21** 058502
[17] Ma Z Y, Chai C C, Ren X R, Yang Y T, Chen B, Song K and Zhao Y B 2012 *Chin. Phys. B* **21** 098502
[18] Ma Z Y, Chai C C, Ren X R, Yang Y T, Zhao Y B and Qiao L P 2013 *Chin. Phys. B* **22** 028502
[19] Wemple S H, Niehous W C, Fukui H, Irvin J C, Cox H M, Hwang J C, Dilorenzo J V and Schlosser W O 1981 *IEEE Trans. Electron Dev.* **28** 834
[20] Whalen J J, Kemerley R and Rastefano E 1982 *IEEE Trans. Micro. Theory Tech.* **30** 2206
[21] Zhang C B, Wang H G, Zhang J D, Du G X and Yang J 2014 *IEEE Trans. Electromagn. Compat.* **56** 1545
[22] Yu X H, Chai C C, Liu Y, Yang Y T and Fan Q Y 2015 *Microelectron. Reliab.* **55** 1174
[23] Zhang C B, Zhang J D, Wang H G and Du G X 2015 *Microelectron. Reliab.* **55** 508
[24] Adachi S *Properties of Gallium Arsenide. EMIS Datareviews Series* (Lodon: Rrozel and G.E.Stillman) p. 32
[25] Blakemore J S 1982 *J. Appl. Phys.* **53** 123
[26] Canali C, Majni G, Minder R and Ottaviani G 1975 *IEEE Trans. Electron Dev.* **22** 1045
[27] Synopsys Inc. 2013 *Sentaurus Device User Guide*, CA, USA
[28] Liu E K, Zhu B S and Luo J S 1994 *The Physics of Semiconductor* (Beijing: National Defense Industry Press), p. 100 (in Chinese)
[29] Chai C C, Yang Y T, Zhang B, Leng P, Yang Y and Rao W 2009 *Semicond. Sci. Technol.* **24** 035003